COO 264-598 EFI 72-2

Addendum to

THE SELF-COUPLING OF WEAK LEPTON CURRENTS IN HIGH ENERGY NEUTRINO AND MUON REACTIONS*

Kazuo Fujikawa

JANUARY, 1972

The Enrico Fermi Institute

The University of Chicago, Chicago, Illinois 60637

ABSTRACT

The transverse momentum distribution of the muons in the reaction $\nu + (z) \rightarrow \nu + \mu + \bar{\mu} + (z)$ is discussed. The lower end of the energy spectrum of the muons in the previous study is also modified by using an improved interpolation formula.

---

*Supported in part by the U. S. Atomic Energy Commission.

Contract No. AT (11-1)-264

DISCLAIMER

In the previous study[1,2] we discussed in detail the energy spectrum of the muons at fixed angle and also angular distributions in the process (see Fig. 1).

$$\nu + (z) \to \nu + \mu + \bar{\mu} + (z) \qquad (1)$$

We also discussed the angular distribution of the muons at fixed energy and energy spectra. Marked asymmetry between μ^- and μ^+ was found, and its origin was discussed.

However we did not discuss the transverse momentum distribution of the muons in the process. In the present note we discuss this transverse momentum distribution based on the calculation reported in the previous study.[1,2] This problem has been discussed by Lovseth and Radomski.[3] It is straightforward to convert the angular distribution at fixed energy in Refs. (1) and (2) into the transverse momentum distribution at fixed energy by using the relation

$$\frac{d^2\sigma}{dE dp_\perp} = \frac{\sin\theta}{|\vec{p}|\cos\theta} \frac{d^2\sigma}{dE d\cos\theta} \qquad (2)$$

where E, $\vec{p}$ and $\cos\theta$ denote the energy, momentum and scattering angle of the muon or the antimuon in the lab. system, respectively. Note that the conversion from the left hand side to the right hand side in Eq. (2) is not so easy due to the singular Jacobian at $\theta = 0$.[4]

We converted Figs. 10, 11, 13 and 14 in Ref. (2) into the transverse momentum distribution.[5] Those resulting distributions are shown in Figs. 2 - 7. Figs. 3 and 5 were newly added to cover the entire range of the muon energy. We also add Figs. 8 and 9. See also the energy spectrum

in Figs. 18 and 19. Our graphs always correspond to single particle inclusive spectra.

In hadron physics it is customary to plot the distribution

$$\frac{d^2\sigma}{dE dp_\perp^2} \equiv \frac{1}{2} \frac{1}{|\vec{p}| \cos\theta} \frac{d^2\sigma}{dE d\cos} \tag{3}$$

In this case the Jacobian is regular around $\theta = 0$. We show the result in Figs. 10 - 13 for an Fe^{56} target and for E_ν = 10 and 40 BeV.

It seems to be that the transverse momentum is not so small, as pointed out by Lovseth and Radomski.[3] This is also qualitativly expected from the momentum transfer from the leptonic system to the nuclear target. The momentum transfer is distributed in the region.

$$t = 10^{-2} \sim 10^{-3} \quad (\text{BeV})^2 \tag{4}$$

See Fig. 19 in Ref. (2), and also Table I in Ref. (3). The value of t in Eq. (4) is about the same as the pion mass squared, $m_\pi^2 = 2 \times 10^{-2}$ $(\text{BeV})^2$. It is generally believed[6] that the finite transverse momentum in the hadronic process is based on the finite (i.e., small) momentum transfer between the particles in the multiperipheral chain. If one takes the pion mass squared as a typical value of the momentum transfer in the hadron process, Eq. (4) suggests that the transverse momentum distribution in the process (1) may not be so distinct from that in hadron processes.

We also show the transverse momentum distribution off a proton target in Figs. 14 and 15, and off a Pb^{208} target in Figs. 16 and 17 for E_ν = 40 BeV. All these calculations are based on the results reported in Ref. (2).[5] These figures, compared with Figs. 2 - 5, clearly indicate the tendency we

just expect. Note that the momentum transfer squared for a proton target is distributed in the region

$$t = 10^{-1} \sim 10^{-3} \quad (\text{BeV})^2 \tag{5}$$

Figs. 14 and 15 suggest that the incoherent process off a proton target may be rather distinct from the semi-leptonic process at high energies. However some model considerations[7] also suggest that the transverse momentum of the secondary particles in the semi-leptonic process may depend on the "mass" of the current. Therefore it is hard to say something definite about the transverse momentum of the hadrons in the semi-leptonic process.[8]

If the Adler process[9] dominates the energetic π^+ production and the "shadow" effect proposed by Bell[10] works in full, the semi-leptonic process would be significantly modified. It is hoped that the detailed experimental study of the semi-leptonic process at high energies will provide us more useful information how to separate the purely leptonic mun production from the background.

Next we would like to correct the lower end of the energy spectra in the previous study.[2] This spectrum was calculated from $\frac{d^2\sigma}{d\cos\theta\, dE}$ at fixed $\cos\theta$ based on an interpolation formula. The conversion of $\frac{d^2\sigma}{d\cos\theta\, dE}$ at $\underline{\text{fixed}}\ \underline{\cos\theta}$ into $\frac{d^2\sigma}{d\cos\theta dE}$ at fixed E was not expected to be so accurate at the lower end of the spectrum.[11] The point is that the integration mesh in the two dimensional phase space ($\cos\theta$, E) was not uniformly taken to achieve the maximum accuracy of the numerical integration. Therefore the conversion from one distribution to the other

is not trivial. However, following the question raised by Llewelyn Smith,[12] we found that the total cross section for an Fe^{56} target at E_ν = 40 BeV obtained from

$$\int \frac{d\sigma}{dE}\, dE \tag{6}$$

grossly exceeds that obtained from

$$\int \frac{d\sigma}{d\cos\theta}\, d\cos\theta \tag{7}$$

Eq. (7) is more or less "exact" in our calculation[1,2]; the values of the total cross section in Refs. (1) and (2) are based on Eq. (7). Therefore the lower end peak in the energy spectrum, in particular, in Fig. 16-b in Ref. (2) is not reliable; this discrepancy goes far beyond what we expected.[11] We show the energy spectra based on an improved interpolation formula in Figs. 18 and 19. These energy spectra differ from the previous values only at below 4% of the lower end of the spectra. See Figs. 15 and 16 in Ref. (2). Fig. 17 in Ref. (2) remains unchanged; this spectrum was calculated by using the exact matrix element. For the sake of completeness we also add the energy spectra off a proton target and also off a Pb^{208} target at E_ν = 40 BeV in Figs. 20 and 21. these graphs show that the muons tend to accumulate near the origin when a larger momentum transfer to the nuclear (or nucleon) system is allowed.

There is also a typographical mistake in the table for total cross sections in Ref. (2). The total cross section for a Pb^{208} target at E_ν = 40 BeV should read

$\sigma(-) = 7.27\ z^2$, $\sigma(+) = 7.16\ z^2$ and $\sigma(a) = 9.6\ z^2$

respectively.

I am grateful to Professors S. B. Treiman and A. Mann for discussions.

References and Footnotes

1. K. Fujikawa, Princeton Thesis, May 1970 (unpublished).

2. K. Fujikawa, Chicago Preprint (1970). To be published in Annals of Physics, December 1971.

3. J. Lovseth and M. Radomski, Phys. Rev. D3, 2686 (1971).

4. Because of this vanishing Jacobian at $\theta = 0$, the sharp peak of the angular distribution at $\theta = 0$ is rather misleading. When one calculates the transverse momentum distribution this sharp peak disappears due to the Jacobian.

5. The computer out-put cards in the previous study which bear the distribution $d^2\sigma/dEd\cos\theta$ for fixed $\cos\theta$ and varying E were used. We converted this distribution into $d^2\sigma/dEd\cos\theta$ for fixed E and varying $\cos\theta$ by an interpolation formula. Then we used Eqs. (2) and (3) to get transverse momentum distributions.

6. See, for example, K. Wilson, Cornell Preprint, CLNS - 131, November (1970).

7. J. D. Bjorken, SLAC-PUB-901 (1971).
K. Fujikawa, Chicago Preprint, EFI-71-69 (1971). To be published in Nuovo Cimento.

8. The transverse momentum of μ^+ in the purely leptonic process could be distinct from that in the semi-leptonic process at extremely high energies because of different particle multiplicity. It is, however, dangerous to discuss this problem further without a detailed knowledge about the transverse momentum in the semi-leptonic process at high energies. If one knows the incident energy of the neutrino, one can form a sort of Dalitz plot for the muon

References and Footnotes (continued)

pair in the final state. In this case it will be slightly easier to distinguish the purely leptonic process from the semi-leptonic process.

9. S. Adler, Phys. Rev. 135, B936 (1964).

10. J. S. Bell, Lecture Note for the 11th Scottish Universities Summer School in Physics, Edinburgh, (1970).

11. We expected that the lower end of the energy spectrum may not be so accurate. See Page 51 of Ref. (1) and also Footnote 20 in Ref. (2). The consistency check of the interpolation formula was made at E_ν = 10 BeV, namely based on Figs. 15 and 17 in Ref. (2). Unfortunately these graphs showed a rather reasonable behavior as one can see by comparing Figs. 18 ~ 21 in the present note with those figures in Ref. (2).

12. C. H. Llewelyn Smith, SLAC Preprint (1971). To be published in Physics Reports.

Figure Captions

Fig. 1. The process $\nu + (z) \rightarrow \nu + \mu + \bar{\mu} + (z)$.

Figs. 2 ~ 5. Transverse momentum distribution $d^2\sigma/dEdp_\perp$ at various energies of the outgoing muons off an Fe^{56} target for E_ν = 40 BeV. Figs. (2) and (4) correspond to Figs. (10) and (11) in Ref. (2). All these graphs represent single particle inclusive spectra.

Figs. 6 and 7. Transverse momentum distribution $d^2\sigma/dEdp_\perp$ off a proton target at E_ν = 10 BeV. These graphs correspond to Figs. (13) and (14) in Ref. (2). $\sigma_0 = 3.03 \times 10^{-44}$ cm^2.

Figs. 8 and 9. Transverse momentum distribution $d^2\sigma/dEdp_\perp$ off an Fe^{56} target at E_ν = 10 BeV. $\sigma_0 = 3.03 \times 10^{-44}$ cm^2.

Figs. 10 and 11. Transverse momentum distribution $d^2\sigma/dEdp_\perp{}^2$ off an Fe^{56} target for E_ν = 10. $\sigma_0 = 3.03 \times 10^{-44}$ cm^2.

Figs. 12 and 13. Transverse momentum distribution $d^2\sigma/dEdp_\perp{}^2$ off an Fe^{56} target for E_ν = 40 BeV. $\sigma_0 = 3.03 \times 10^{-44}$ cm^2.

Figs. 14 and 15. Transverse momentum distribution $d^2\sigma/dEdp_\perp$ off a proton target at E_ν = 40 BeV. $\sigma_0 = 3.03 \times 10^{-44}$ cm^2.

Figs. 16 and 17. Transverse momentum distribution $d^2\sigma/dEdp_\perp$ off a Pb^{208} target at E_ν = 40 BeV. $\sigma_0 = 3.03 \times 10^{-44}$ cm^2.

Fig. 18. Energy spectrum $d\sigma/dE$ off an Fe^{56} target at E_ν = 10 BeV. This diagram corresponds to Fig. 15 in Ref. (2). $\sigma_0 = 3.03 \times 10^{-44}$ cm^2.

Fig. 19. Energy spectrum $d\sigma/dE$ off an Fe^{56} target at E_ν = 40 BeV. This diagram corresponds to Fig. 16 in Ref. (2). $\sigma_0 = 3.03 \times 10^{-44}$ cm^2.

Fig. 20. Energy spectrum $d\sigma/dE$ off a proton target at E_ν = 40 BeV. $\sigma_0 = 3.03 \times 10^{-44}$ cm^2.

Figure Captions (continued)

Fig. 21. Energy spectrum $d\sigma/dE$ off a Pb^{208} target at E_ν = 40 BeV. $\sigma_0 = 3.03 \times 10^{-44}$ cm^2.

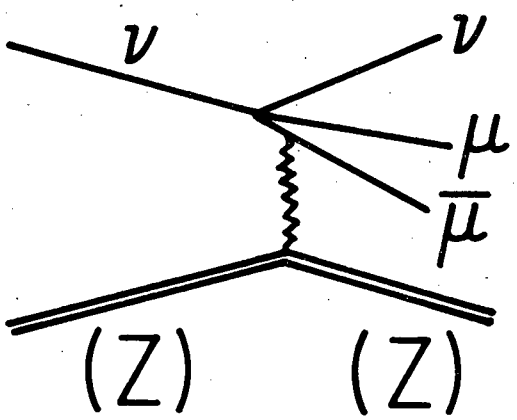

Fig. 1

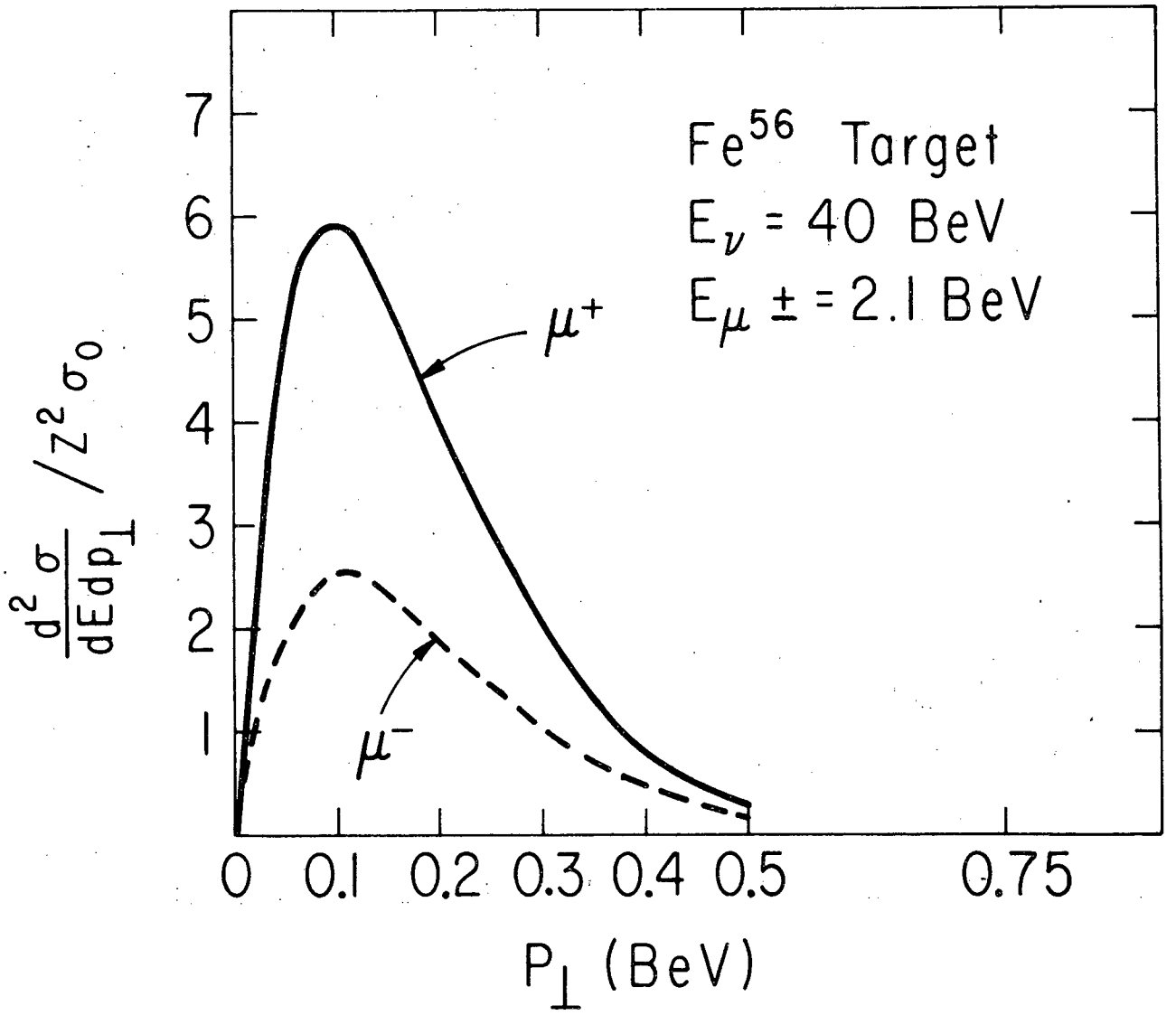
Fe^{56} Target
E_ν = 40 BeV
$E_\mu \pm$ = 2.1 BeV
μ^+
μ^-
$\frac{d^2\sigma}{dEdp_\perp} / Z^2\sigma_0$
7
6
5
4
3
2
1
0
0.1
0.2
0.3
0.4
0.5
0.75
$P_\perp$ (BeV)

Fig.2

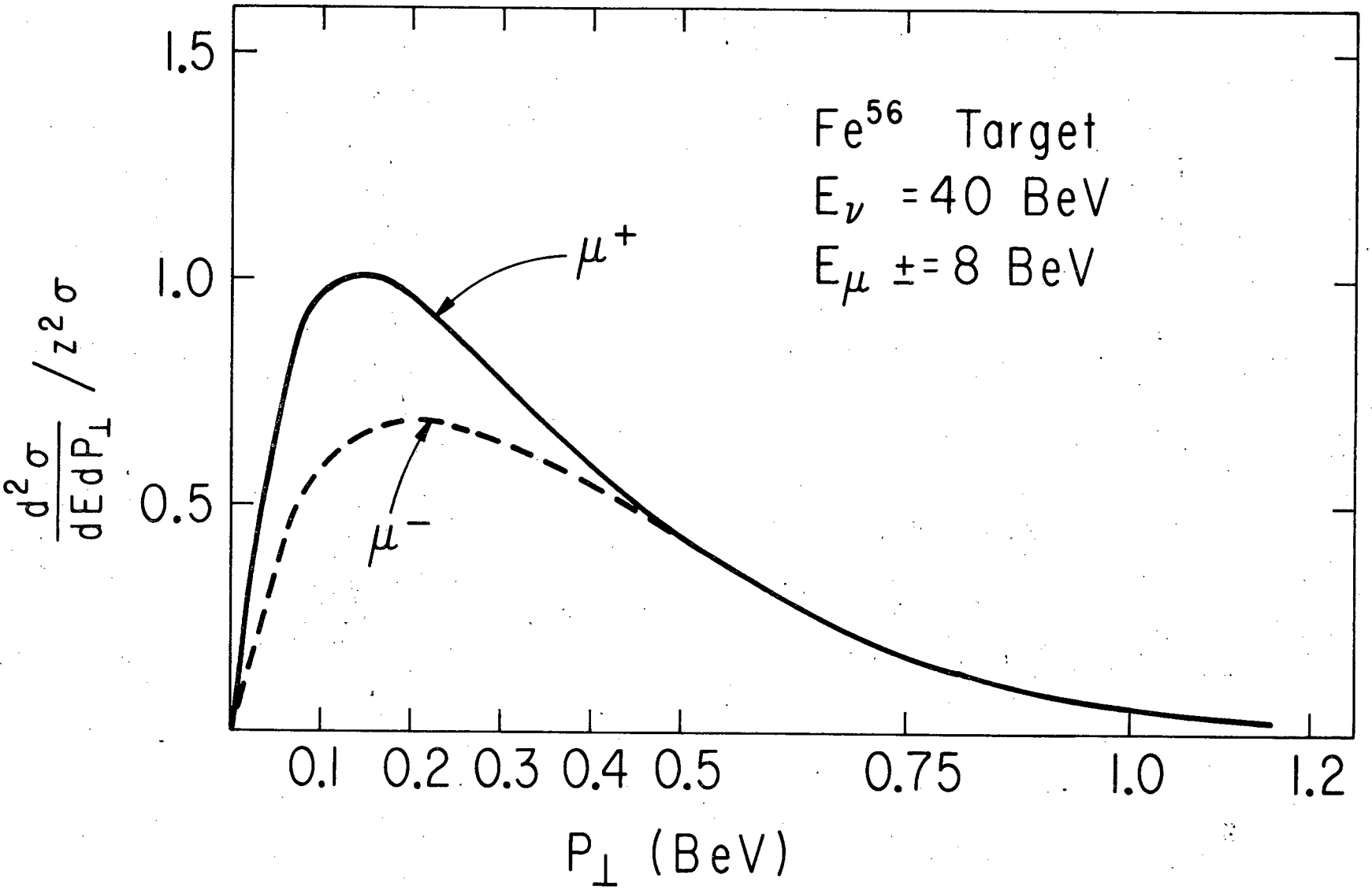
1.5
1.0
0.5
$\frac{d^2\sigma}{dE\,dP_\perp} / z^2\sigma$
Fe^{56} Target
E_ν = 40 BeV
$E_\mu \pm$ = 8 BeV
μ^+
μ^-
0.1 0.2 0.3 0.4 0.5 0.75 1.0 1.2
$P_\perp$ (BeV)

Fig.3

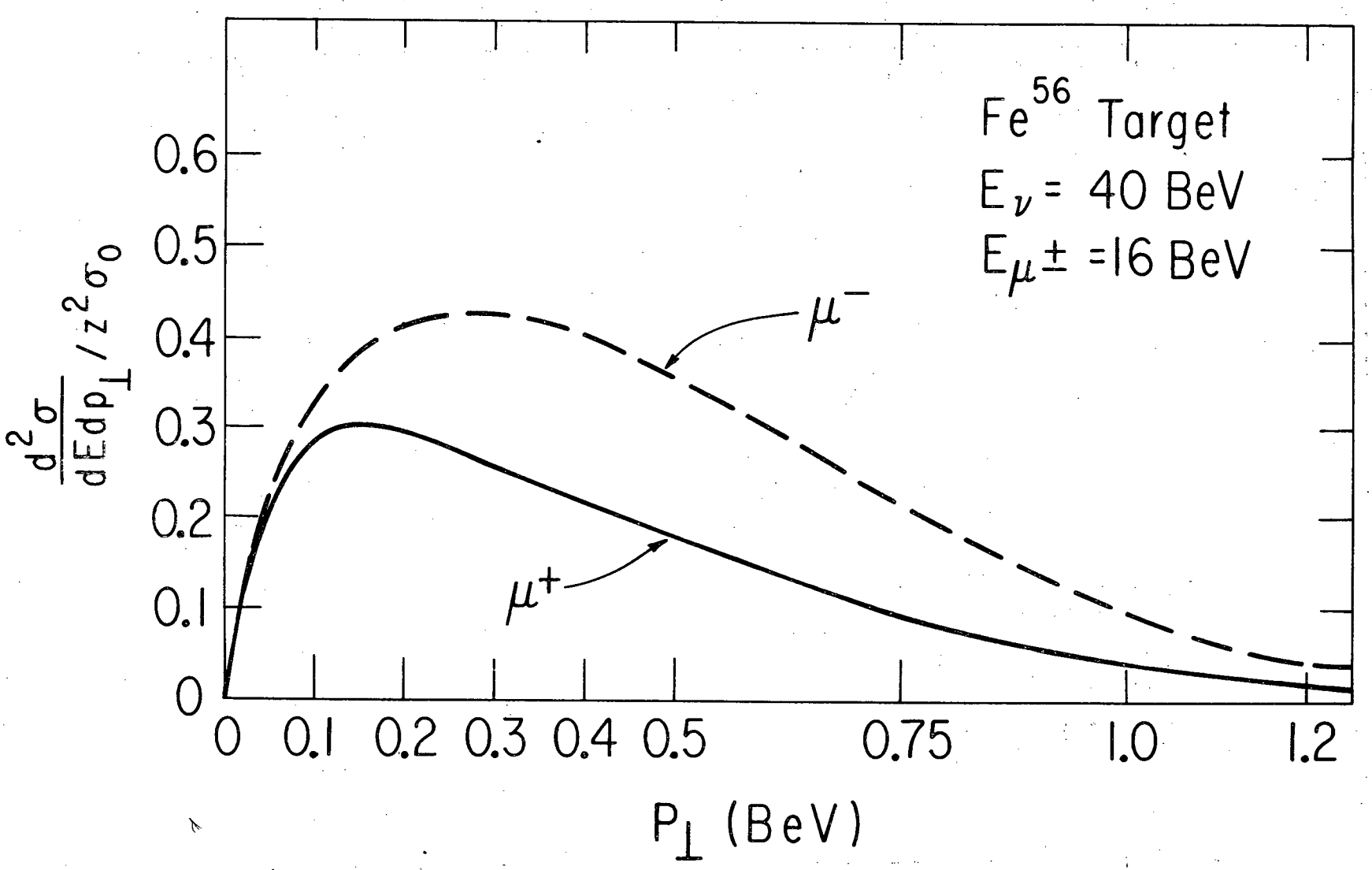
Fe^{56} Target
E_ν = 40 BeV
$E_{\mu\pm}$ = 16 BeV
μ^-
μ^+
$\frac{d^2\sigma}{dE dp_\perp} / z^2\sigma_0$
0
0.1
0.2
0.3
0.4
0.5
0.6
0
0.1
0.2
0.3
0.4
0.5
0.75
1.0
1.2
$P_\perp$ (BeV)

Fig.4

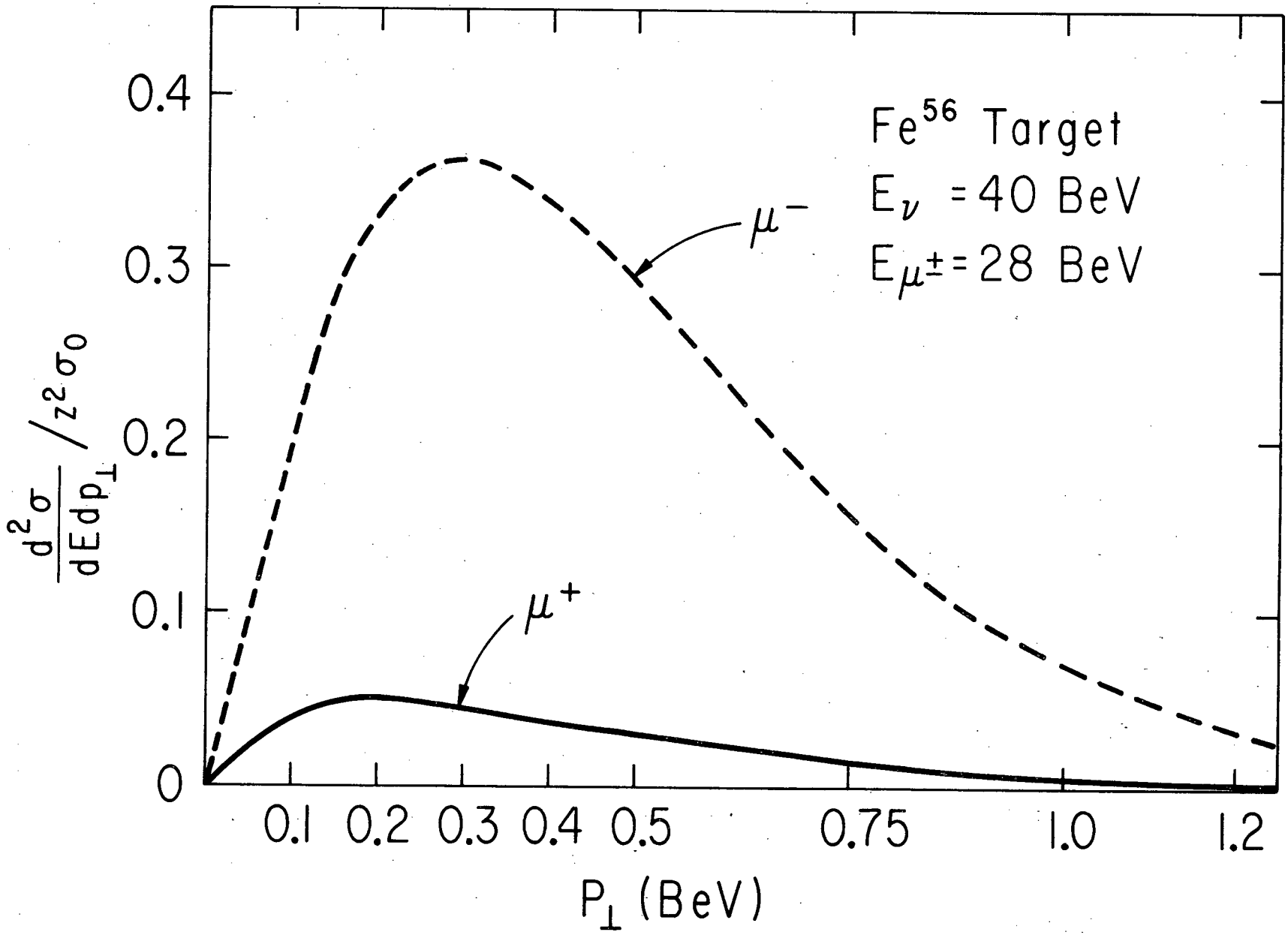
0.4
0.3
0.2
0.1
0
$\frac{d^2\sigma}{dE\,dp_\perp} / z^2\sigma_0$
Fe^{56} Target
E_ν = 40 BeV
$E_{\mu^\pm}$ = 28 BeV
μ^-
μ^+
0.1 0.2 0.3 0.4 0.5 0.75 1.0 1.2
$P_\perp$ (BeV)

Fig.5

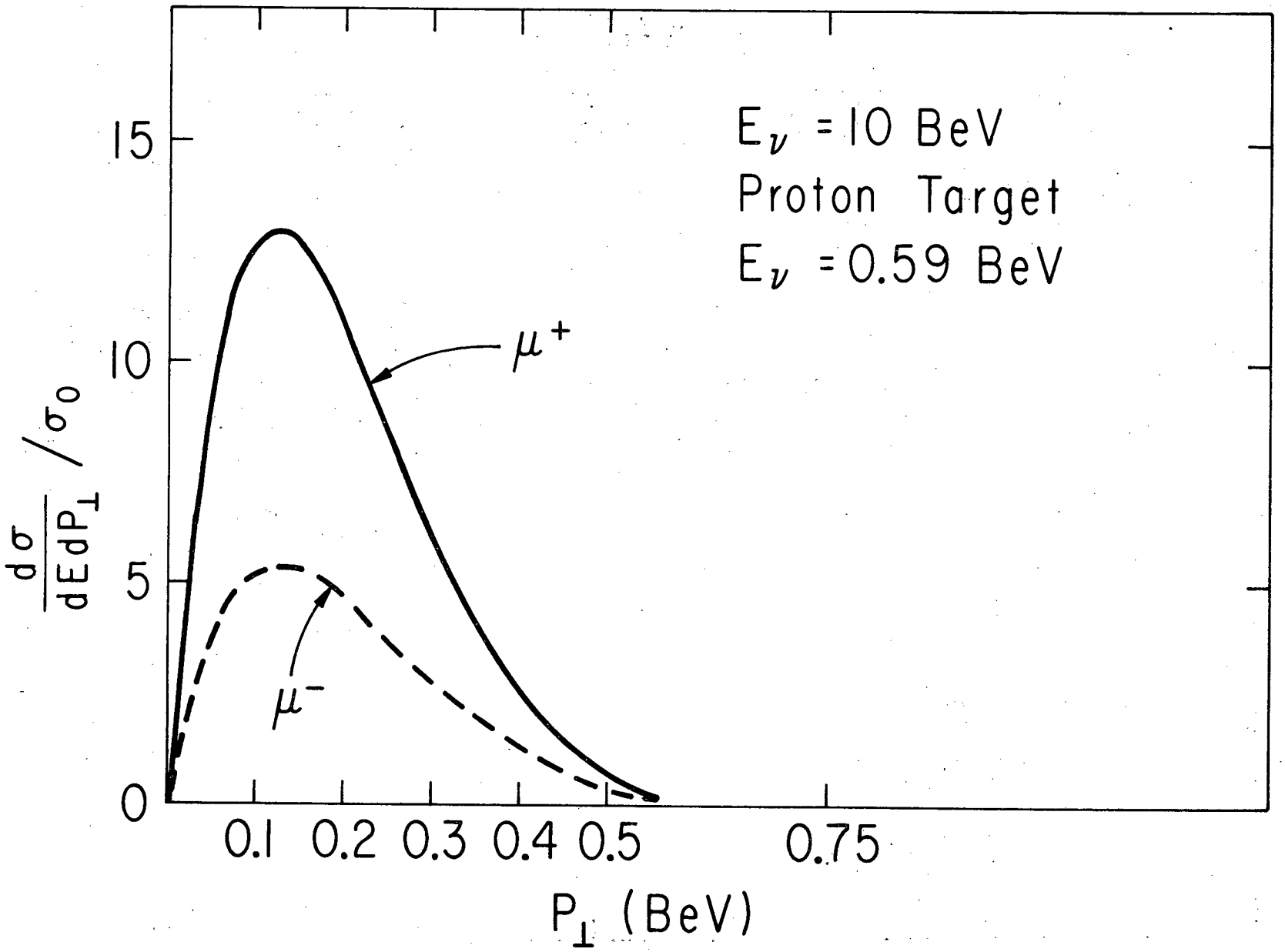
E_ν = 10 BeV
Proton Target
E_ν = 0.59 BeV
μ^+
μ^-
$\frac{d\sigma}{dE dP_\perp} / \sigma_0$
15
10
5
0
0.1
0.2
0.3
0.4
0.5
0.75
$P_\perp$ (BeV)

Fig.6

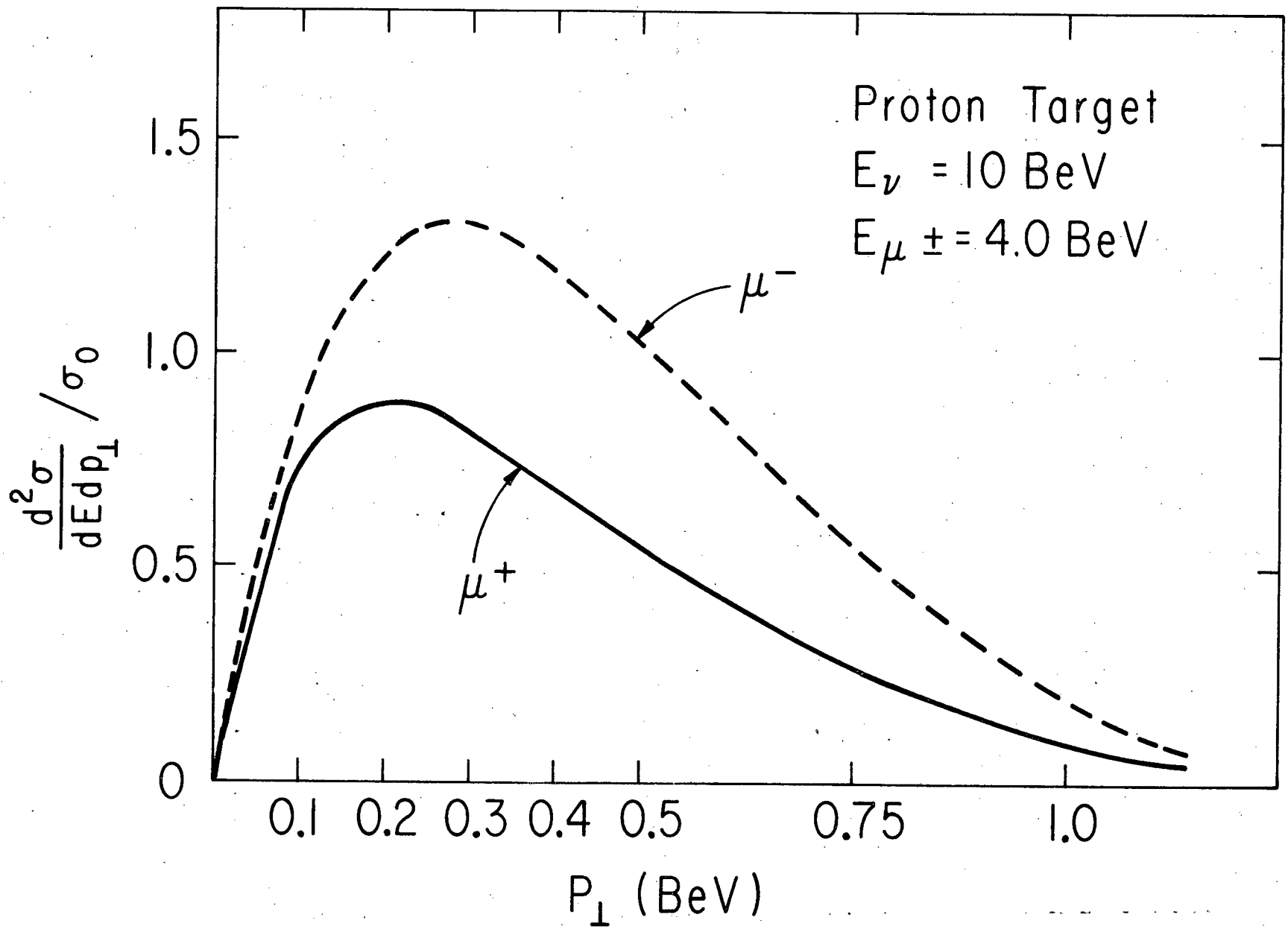
Proton Target
E_ν = 10 BeV
$E_\mu \pm$ = 4.0 BeV
μ^-
μ^+
$\frac{d^2\sigma}{dE\,dp_\perp} / \sigma_0$
1.5
1.0
0.5
0
0.1
0.2
0.3
0.4
0.5
0.75
1.0
$P_\perp$ (BeV)

Fig.7

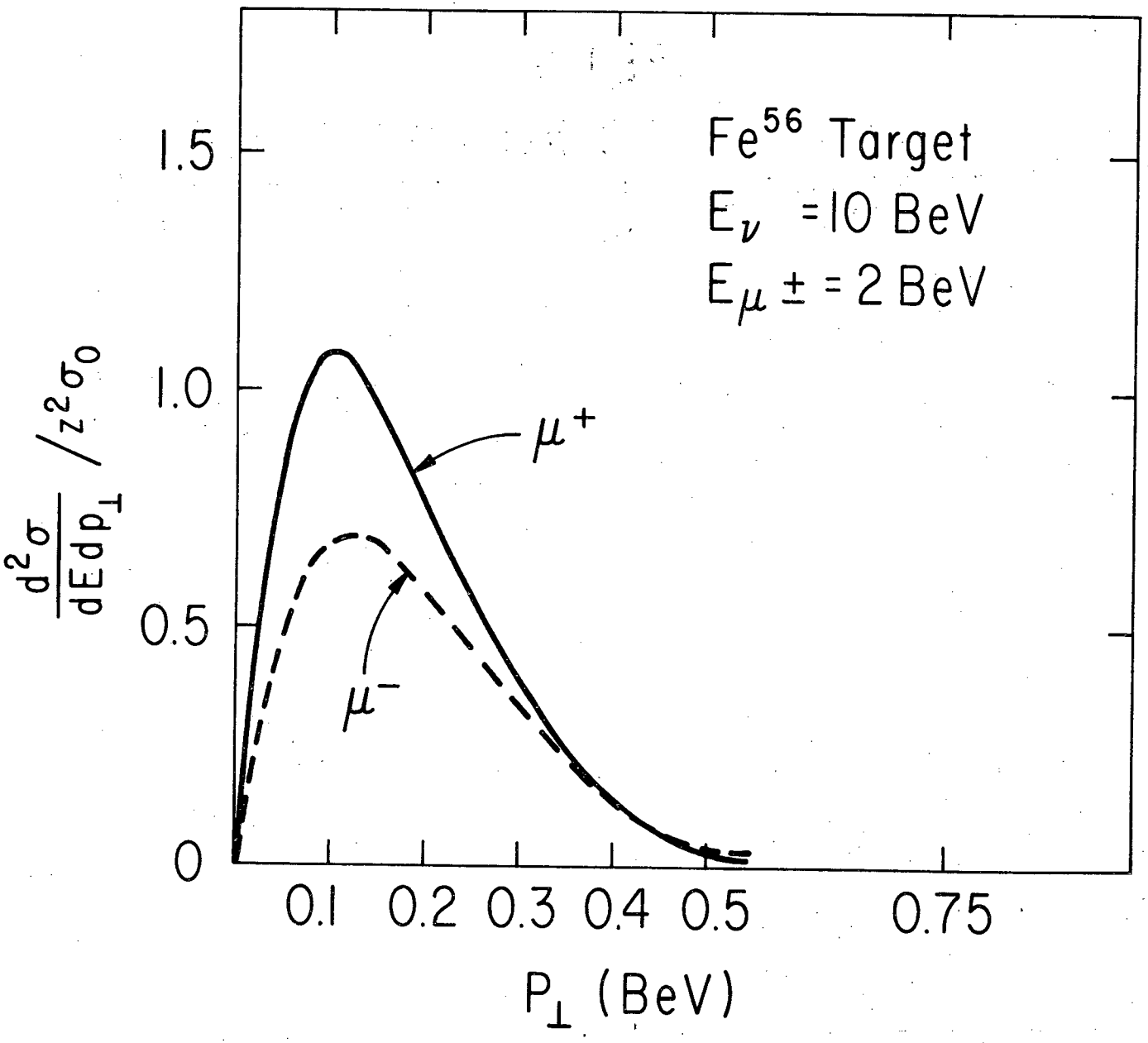
Fe56 Target
Eν =10 BeV
Eμ ± = 2 BeV
μ+
μ−
1.5
1.0
0.5
0
0.1
0.2
0.3
0.4
0.5
0.75
P⊥ (BeV)
d²σ / dE dp⊥ /z²σ₀

Fig.8

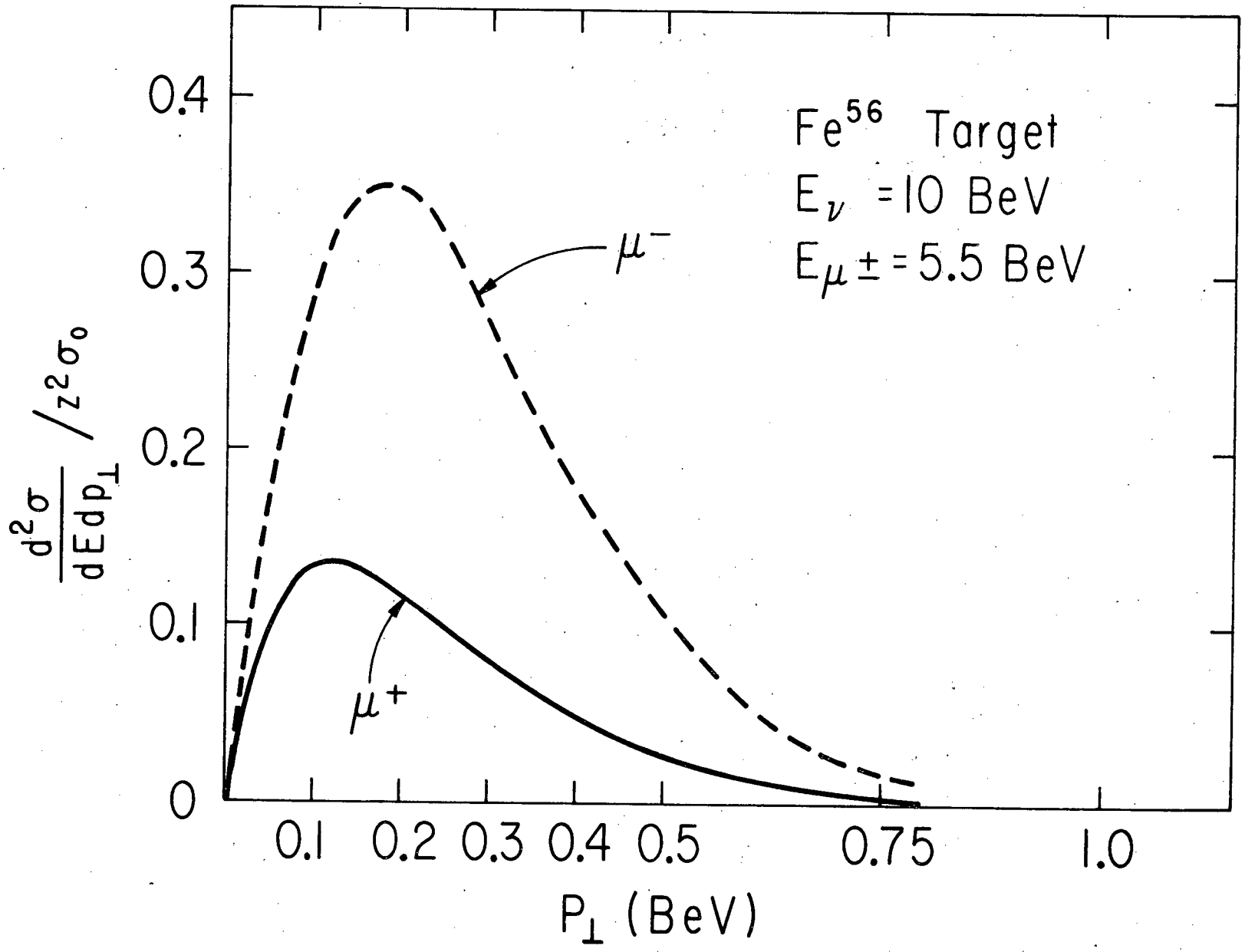
Fe^{56} Target
E_ν = 10 BeV
$E_{\mu\pm}$ = 5.5 BeV
μ^-
μ^+
$\frac{d^2\sigma}{dE dp_\perp} / z^2\sigma_o$
0
0.1
0.2
0.3
0.4
0.1
0.2
0.3
0.4
0.5
0.75
1.0
$P_\perp$ (BeV)

Fig. 9

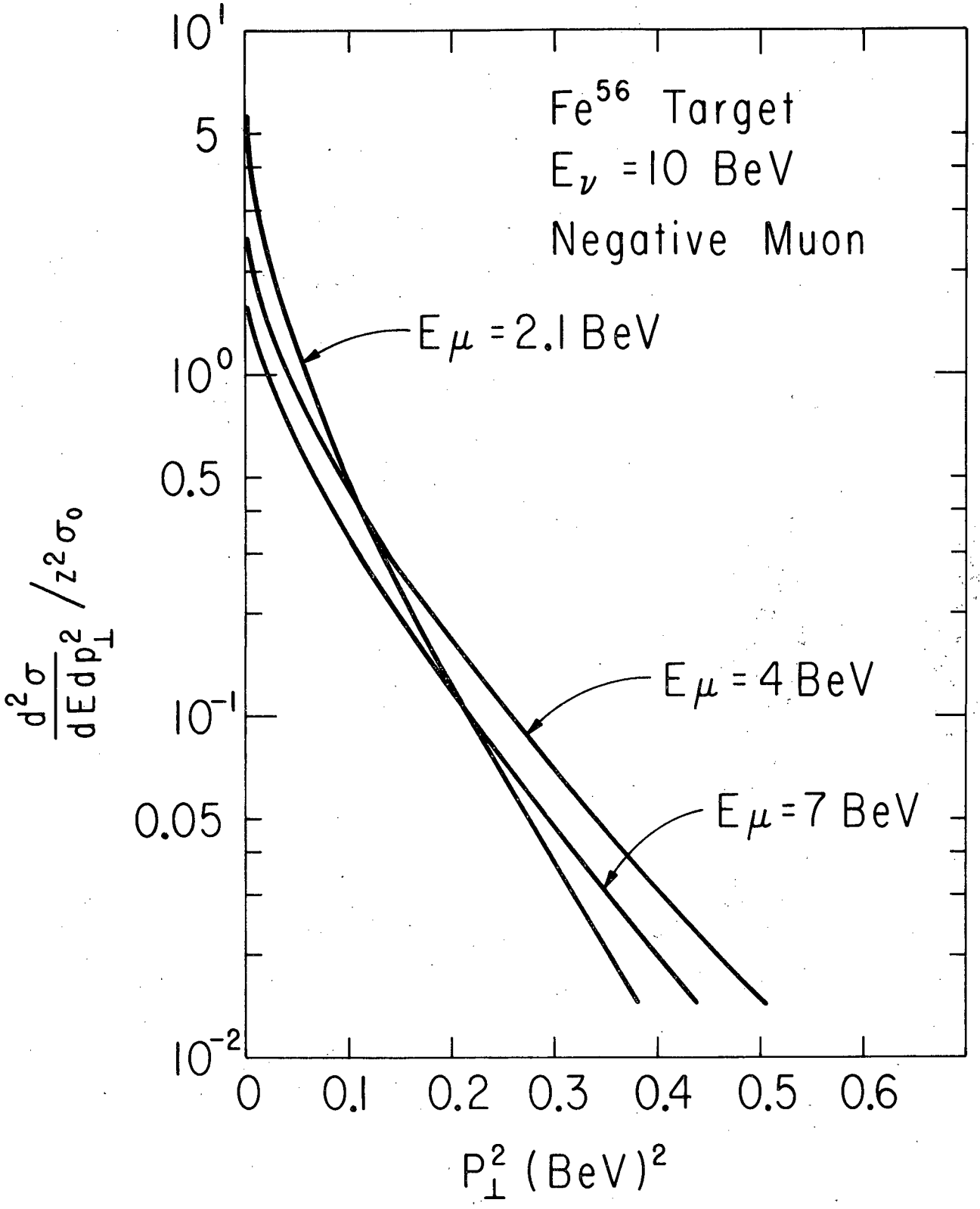
Fe56 Target
Eν =10 BeV
Negative Muon
Eμ =2.1 BeV
Eμ =4 BeV
Eμ =7 BeV
10¹
5
10⁰
0.5
10⁻¹
0.05
10⁻²
0
0.1
0.2
0.3
0.4
0.5
0.6
P⊥² (BeV)²
d²σ/dE dp⊥² /z²σ₀

Fig.10

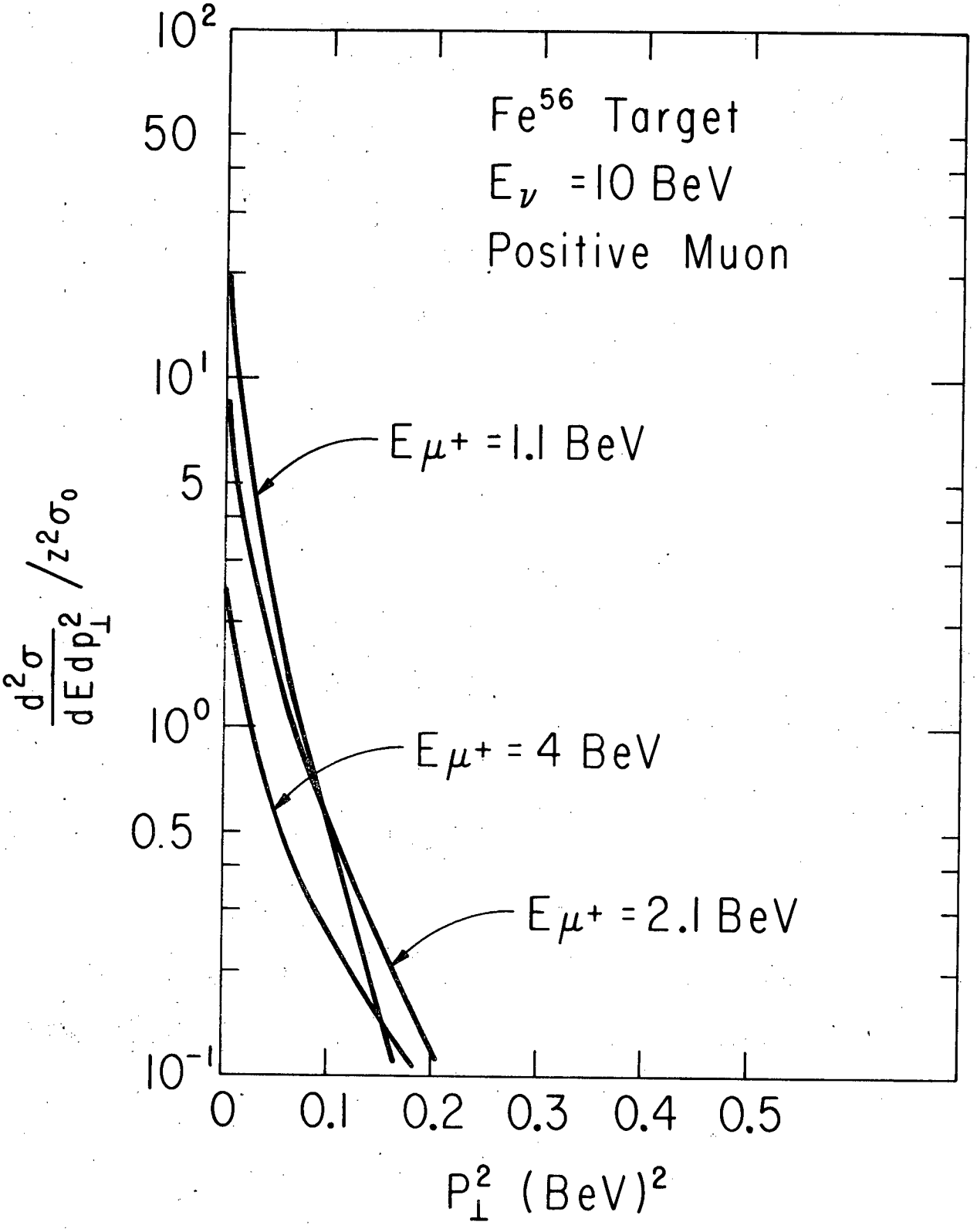
10^2
50
10^1
5
10^0
0.5
10^{-1}
Fe^{56} Target
E_ν = 10 BeV
Positive Muon
$E\mu^+$ = 1.1 BeV
$E\mu^+$ = 4 BeV
$E\mu^+$ = 2.1 BeV
$\frac{d^2\sigma}{dE\,dp_\perp^2} / z^2\sigma_0$
0
0.1
0.2
0.3
0.4
0.5
$P_\perp^2$ (BeV)^2

Fig.11

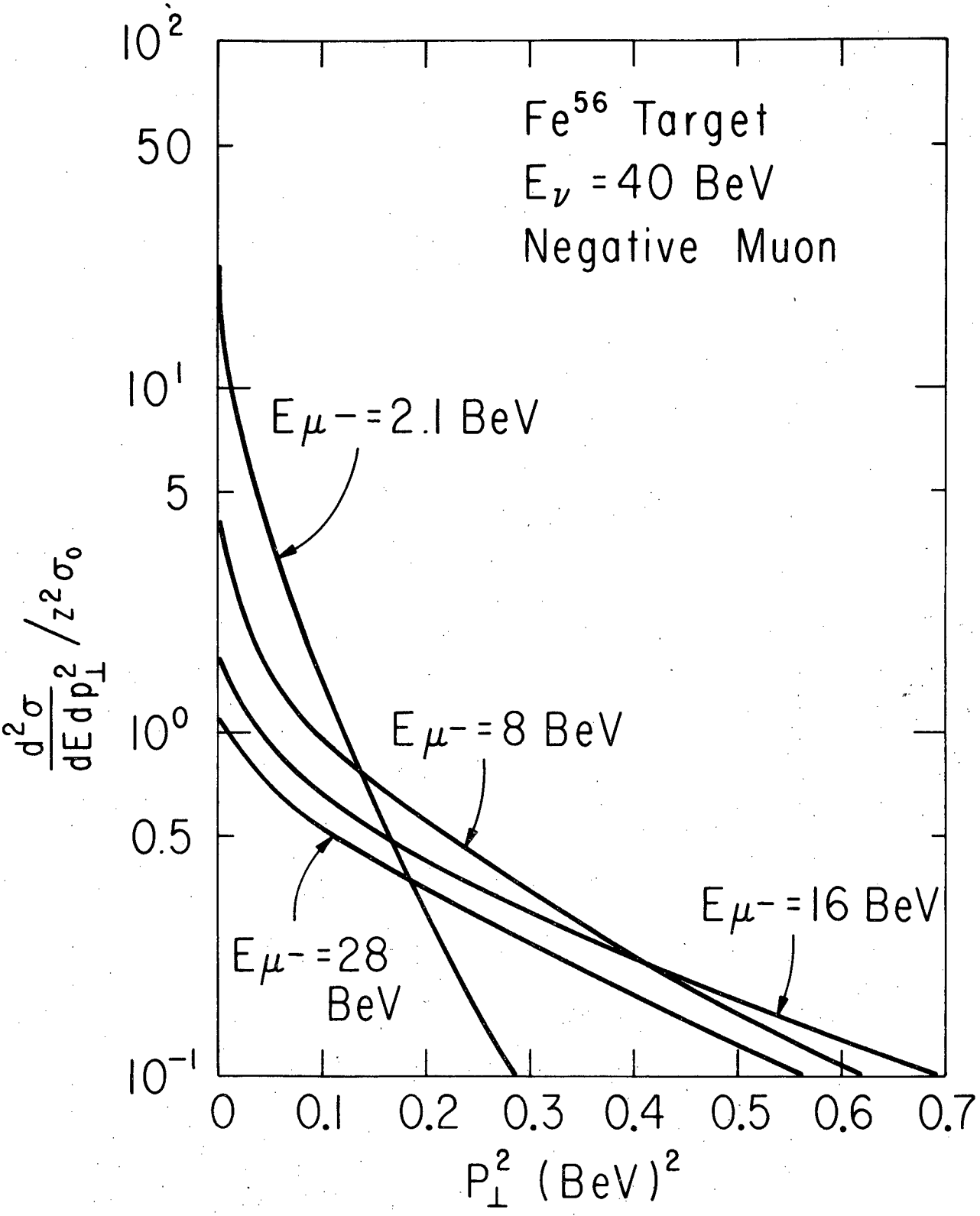
10^2
50
10^1
5
10^0
0.5
10^{-1}
$\frac{d^2\sigma}{dE\,dp_\perp^2}/z^2\sigma_0$
Fe^{56} Target
E_ν = 40 BeV
Negative Muon
$E\mu^-$ = 2.1 BeV
$E\mu^-$ = 8 BeV
$E\mu^-$ = 16 BeV
$E\mu^-$ = 28 BeV
0
0.1
0.2
0.3
0.4
0.5
0.6
0.7
$P_\perp^2$ (BeV)^2

Fig. 12

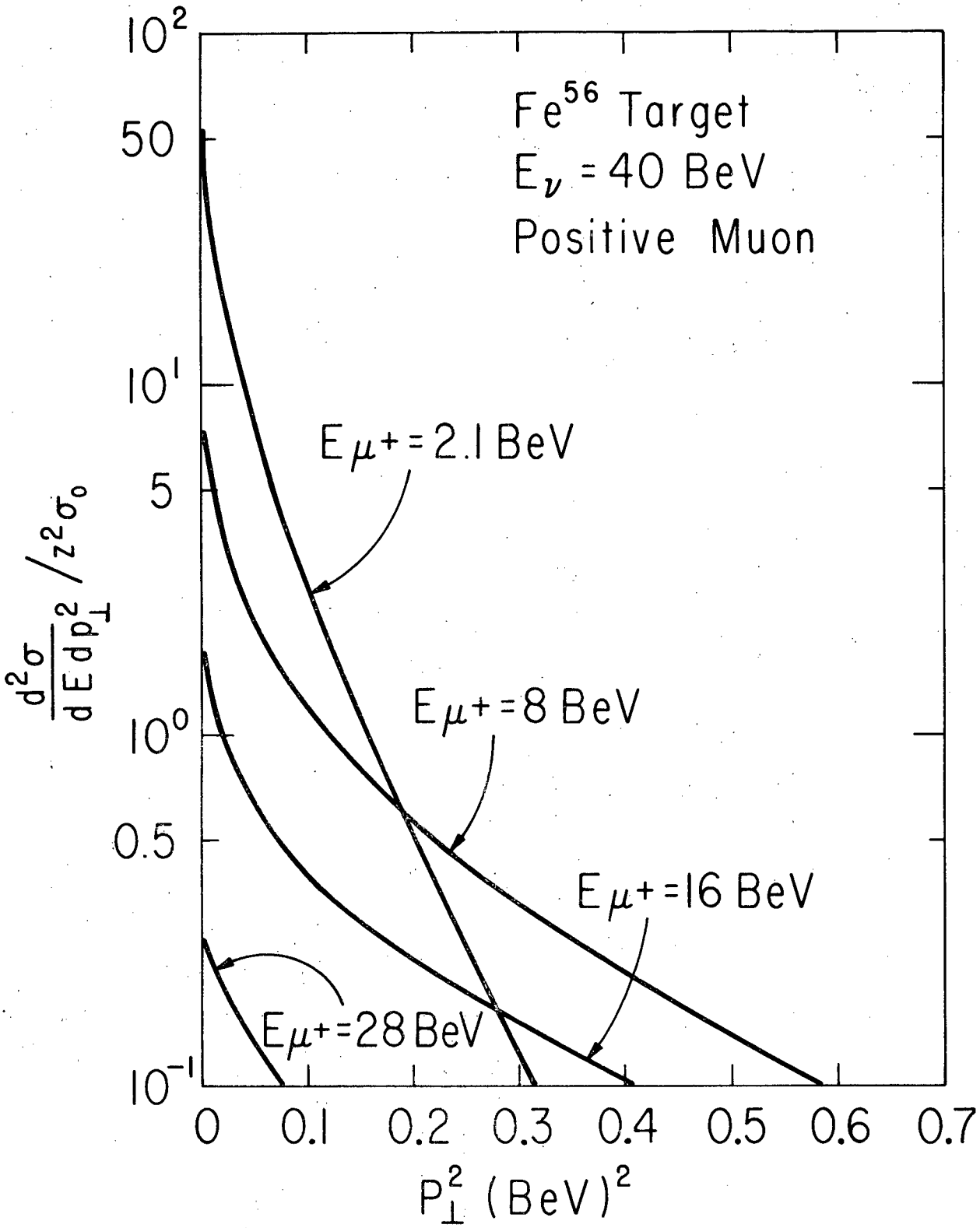
10^2
50
10^1
5
10^0
0.5
10^{-1}
$\frac{d^2\sigma}{dE\,dp_\perp^2}/z^2\sigma_0$
Fe^{56} Target
E_ν = 40 BeV
Positive Muon
$E\mu^+$ = 2.1 BeV
$E\mu^+$ = 8 BeV
$E\mu^+$ = 16 BeV
$E\mu^+$ = 28 BeV
0
0.1
0.2
0.3
0.4
0.5
0.6
0.7
$P_\perp^2$ (BeV)^2

Fig.13

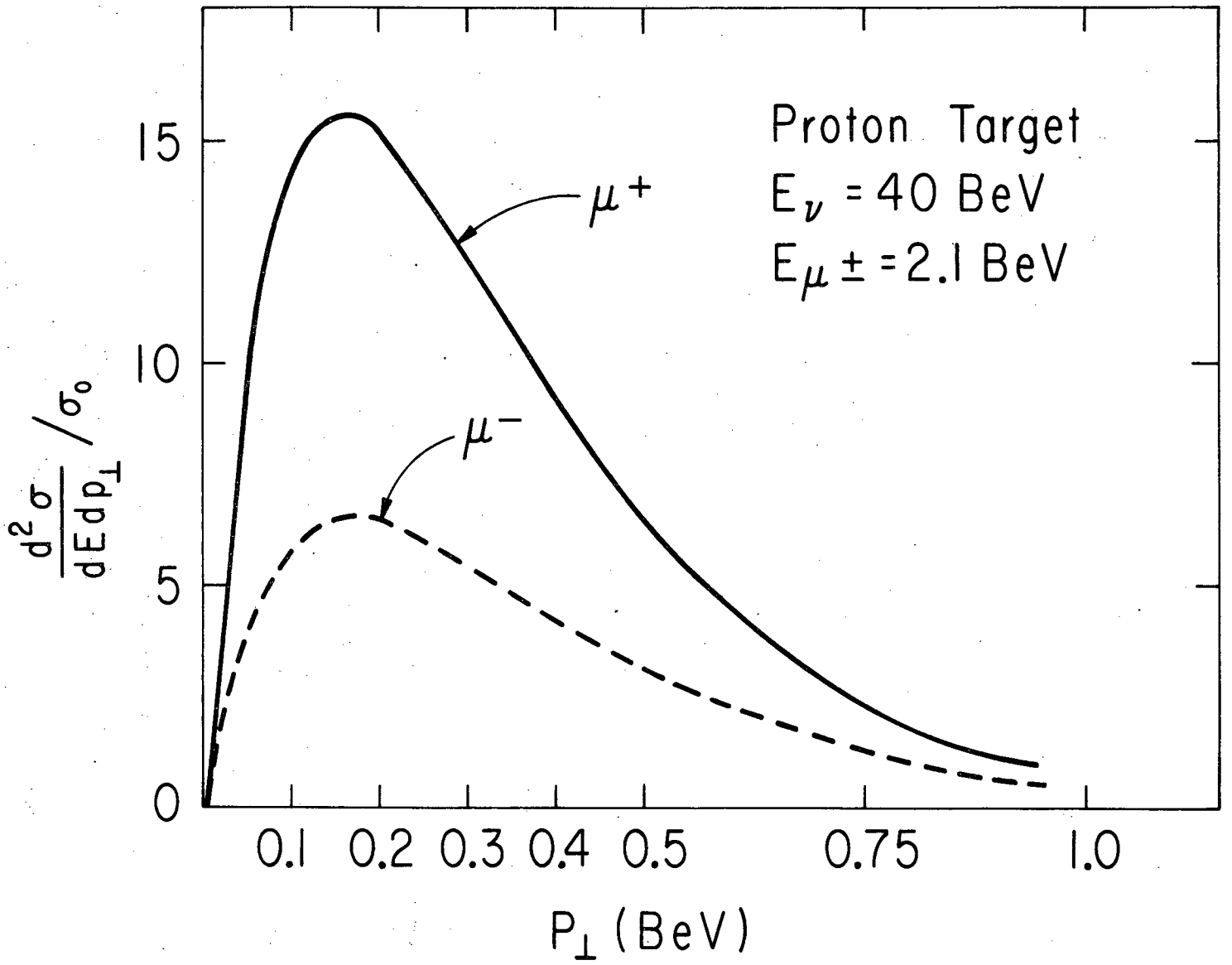
Proton Target
E_ν = 40 BeV
$E_{\mu\pm}$ = 2.1 BeV
μ^+
μ^-
$\frac{d^2\sigma}{dE\,dp_\perp}/\sigma_0$
15
10
5
0
0.1
0.2
0.3
0.4
0.5
0.75
1.0
$P_\perp$ (BeV)

Fig.14

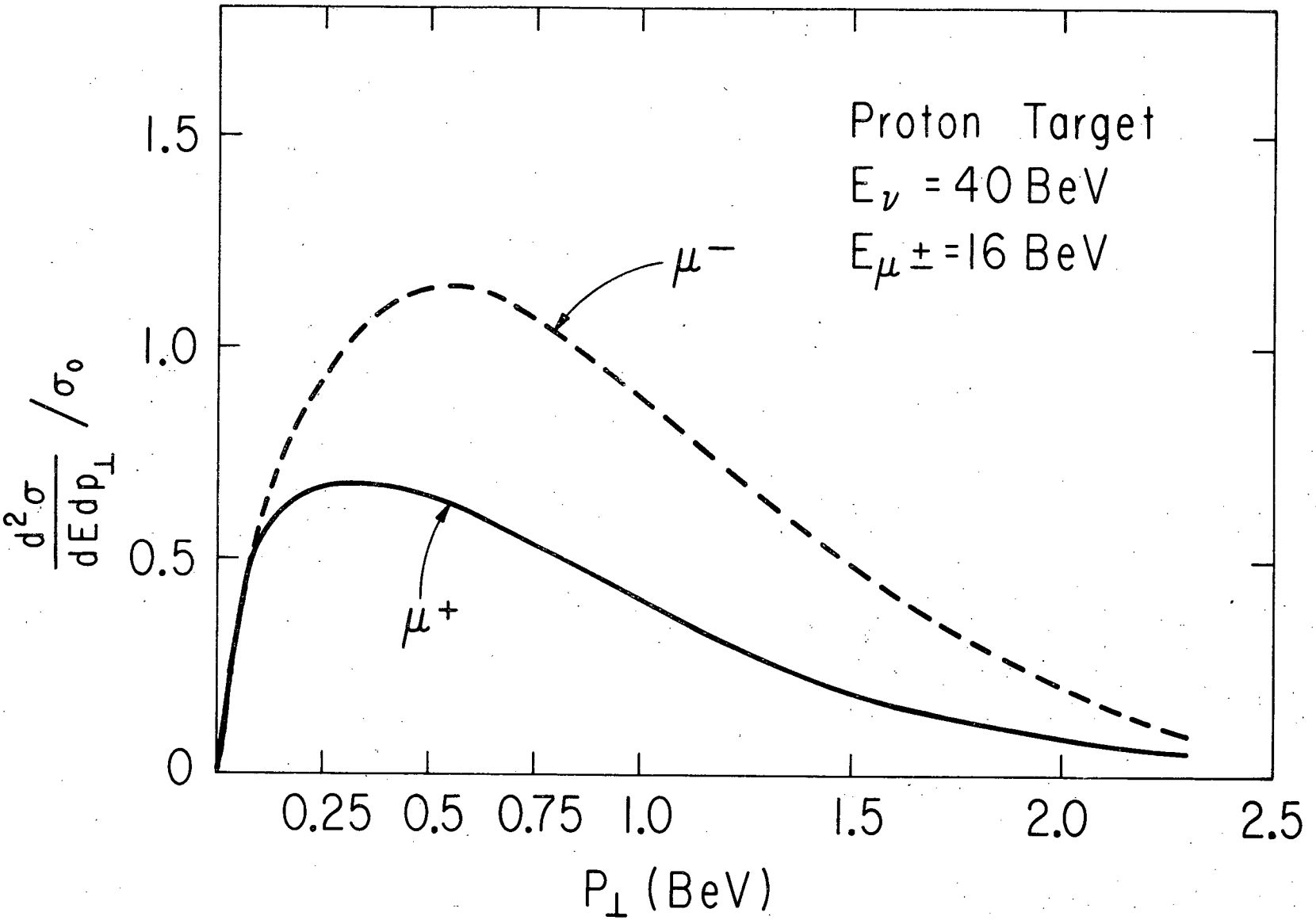
Proton Target
E_ν = 40 BeV
$E_{\mu\pm}$ = 16 BeV
μ^-
μ^+
$\frac{d^2\sigma}{dE\,dp_\perp} / \sigma_0$
1.5
1.0
0.5
0
0.25
0.5
0.75
1.0
1.5
2.0
2.5
$P_\perp$ (BeV)

Fig. 15

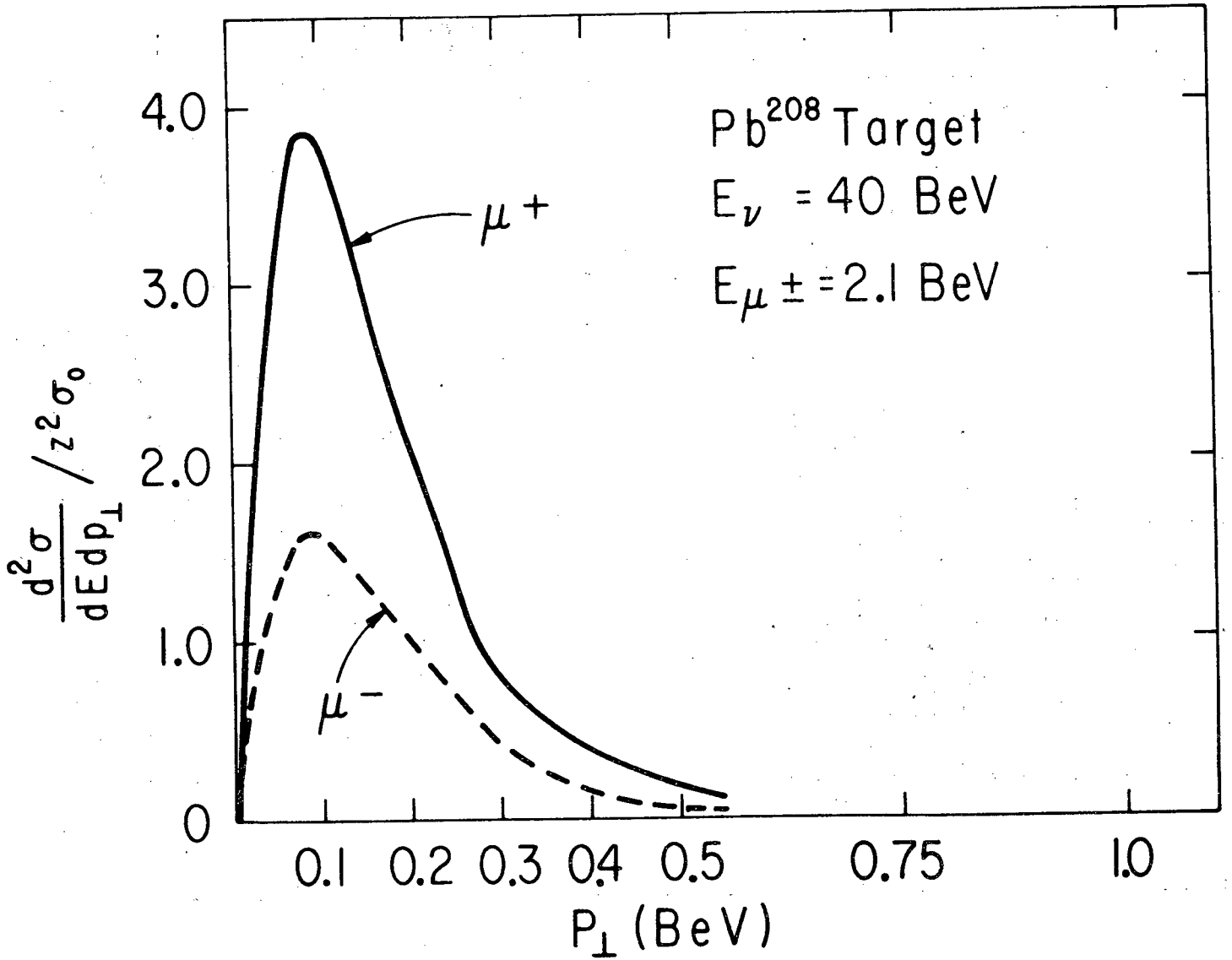
4.0
3.0
2.0
1.0
0
$\frac{d^2\sigma}{dE\,dp_\perp} / z^2\sigma_o$
Pb^{208} Target
E_ν = 40 BeV
$E_{\mu\pm}$ = 2.1 BeV
μ^+
μ^-
0.1
0.2
0.3
0.4
0.5
0.75
1.0
$P_\perp$ (BeV)

Fig. 16

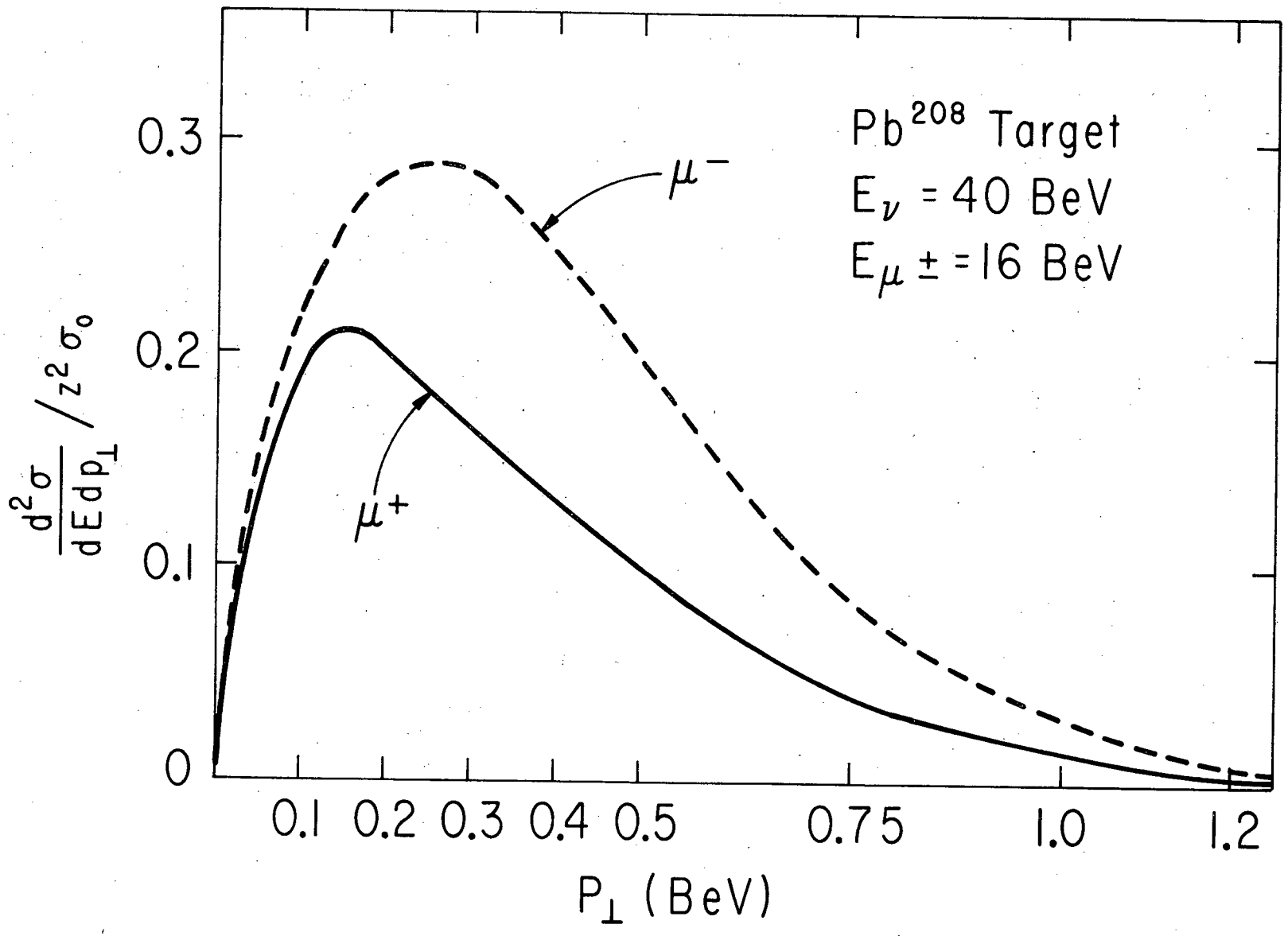
Pb^{208} Target
E_ν = 40 BeV
$E_\mu \pm$ = 16 BeV
μ^-
μ^+
$\frac{d^2\sigma}{dE\,dp_\perp} / z^2\sigma_0$
0
0.1
0.2
0.3
0.1 0.2 0.3 0.4 0.5 0.75 1.0 1.2
$P_\perp$ (BeV)

Fig.17

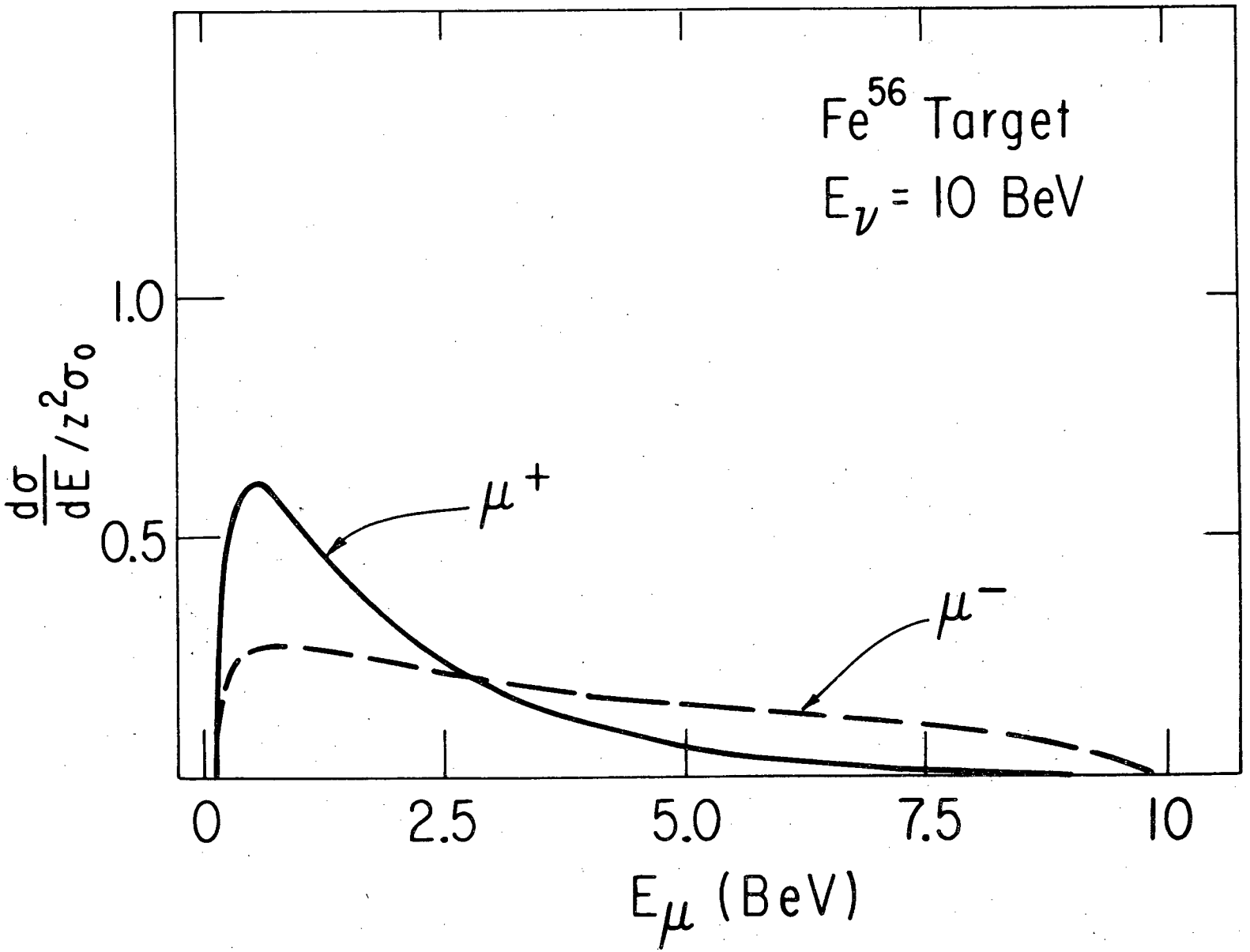

Fig.18

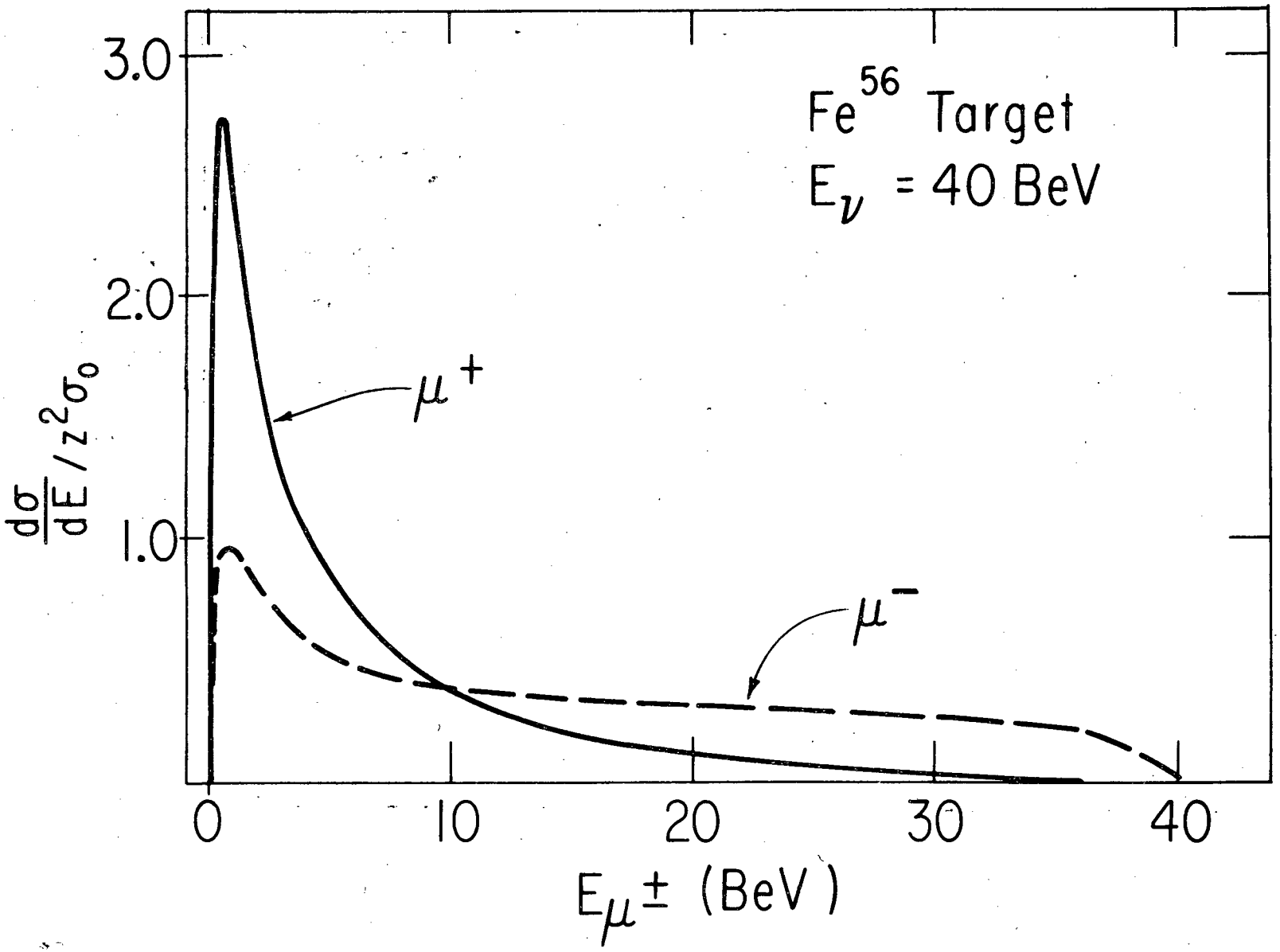
3.0
2.0
1.0
$\frac{d\sigma}{dE}/z^2\sigma_0$
Fe^{56} Target
E_ν = 40 BeV
μ^+
μ^-
0
10
20
30
40
$E_{\mu^\pm}$ (BeV)

Fig.19

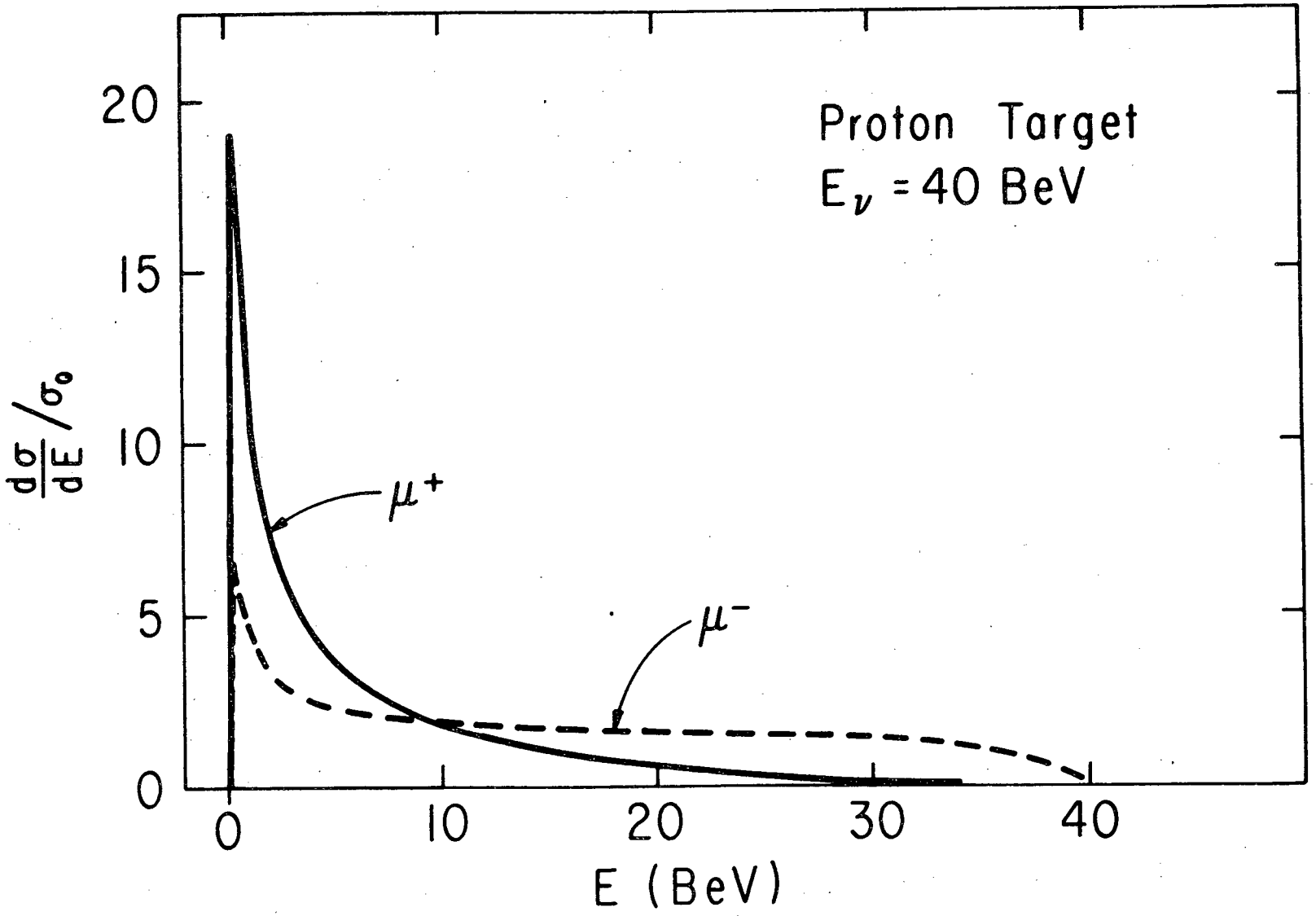
Proton Target
E_ν = 40 BeV
μ^+
μ^-
$\frac{d\sigma}{dE}/\sigma_o$
0
5
10
15
20
0
10
20
30
40
E (BeV)

Fig.20

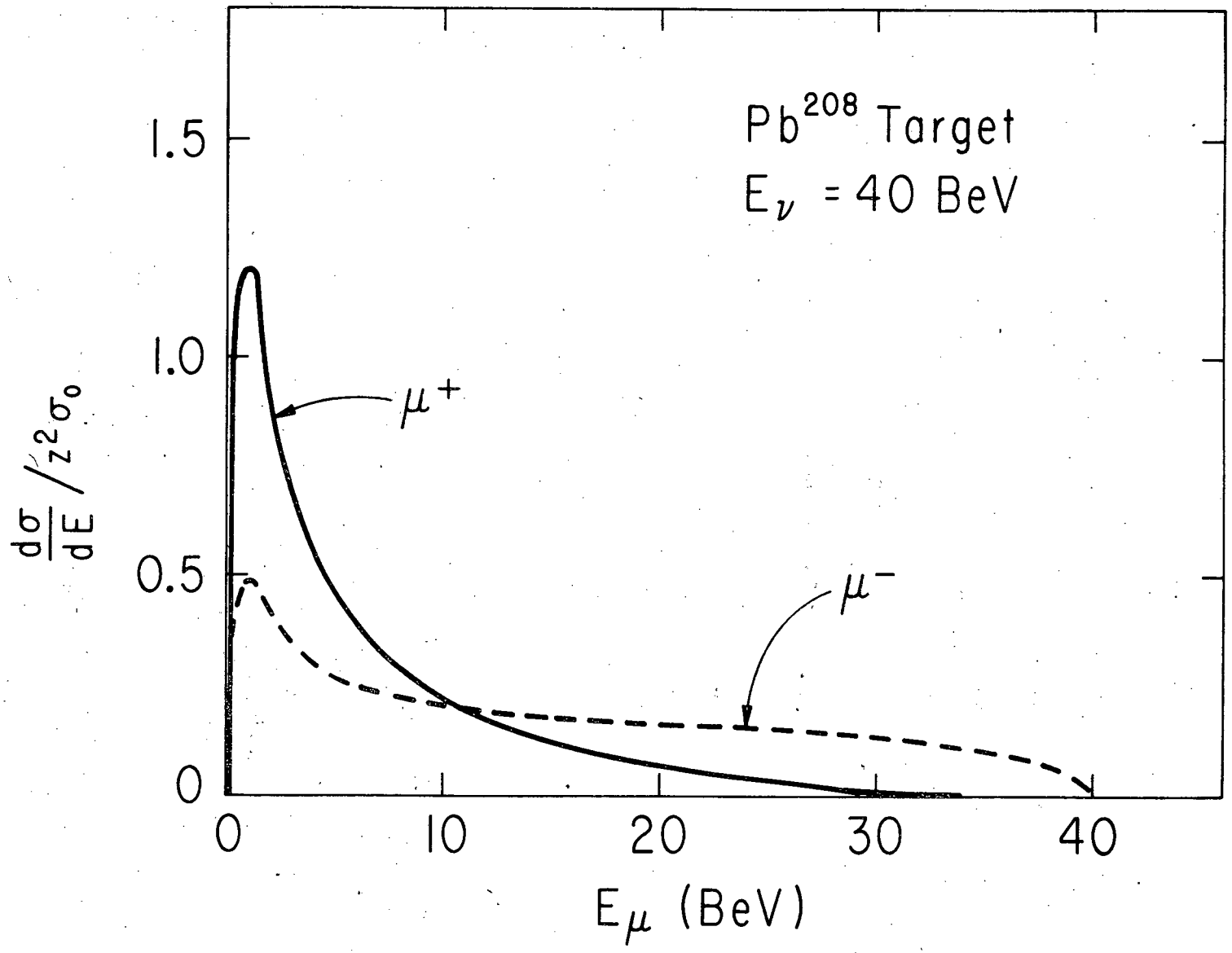
Pb^{208} Target
E_ν = 40 BeV
μ^+
μ^-
$\frac{d\sigma}{dE}/Z^2\sigma_0$
1.5
1.0
0.5
0
0
10
20
30
40
E_μ (BeV)

Fig. 21